DOI: 10.1002/anie.201407468

Theranostic Iridium Complexes

Theranostic Iridium(III) Complexes as One- and Two-Photon Phosphorescent Trackers to Monitor Autophagic Lysosomes**

Liang He, Cai-Ping Tan, Rui-Rong Ye, Yi-Zhi Zhao, Ya-Hong Liu, Qiang Zhao, Liang-Nian Ji, and Zong-Wan Mao**

Abstract: *During autophagy, the intracellular components are captured in autophagosomes and delivered to lysosomes for degradation and recycling. Changes in lysosomal trafficking and contents are key events in the regulation of autophagy, which has been implicated in many physiological and pathological processes. In this work, two iridium(III) complexes (**LysoIr1** and **LysoIr2**) are developed as theranostic agents to monitor autophagic lysosomes. These complexes display lysosome-activated phosphorescence and can specifically label lysosomes with high photostability. Simultaneously, they can induce autophagy potently without initiating an apoptosis response. We demonstrate that **LysoIr2** can effectively implement two functions, namely autophagy induction and lysosomal tracking, in the visualization of autophagosomal–lysosomal fusion. More importantly, they display strong two-photon excited fluorescence (TPEF), which is favorable for live cell imaging and in vivo applications.*

Lysosomes (pH 4.5–5.5) and endosomes (pH 4.5–6.8) are acidic organelles that play essential roles in many physiological processes and cell signaling pathways, including intracellular transportation, protein degradation and recycling, cell membrane recycling, endocytosis, apoptosis as well as autophagy.[1] It is noteworthy that autophagy is a lysosomal degradation pathway that plays important roles in the cellular and tissue homeostasis, physiology, development, and also in the prevention and treatment of human diseases.[2] During autophagy, cytoplasmic materials and damaged organelles are engulfed in autophagosomes, after which the autophagosomes fuse with lysosomes to acquire acidic hydrolases for cargo degradation.[3] Lysosomes are very critical subcellular organelles to execute the autophagic process. Changes in lysosomal trafficking and contents account for the regulation of autophagy, in particular through the aberrant cellular release of a class of proteases.[4] It has been reported that lysosomes increase in number, acidity, and size during autophagy.[5] Real-time tracking of lysosomes can help us to better understand the lysosome-associated events during autophagy, e.g., release of lysosomal proteases, autophagosome maturation, and fusion of lysosomes with other organelles.

Recently, much research effort has been devoted to developing sensitive and specific lysosomal probes for understanding the roles of lysosomes in cellular processes.[6] The tracking of lysosomes during the autophagic process is of particular concern. Lysosomes are often labeled with the lysosome-associated membrane protein-2 (LAMP-2) or commercially available lysosomal probes. Simultaneously, autophagy is stimulated by starvation or autophagy-inducing agents.[5,7] Because it is difficult to avoid nonspecific interactions between different staining and inducing agents, multifunctional theranostic agents cannot only greatly facilitate the whole process but also provide more reliable experimental results.

As demonstrated by the groups of Sadler and Meggers, iridium complexes are very promising alternatives to platinum-based metallo-anticancer drugs.[8] Meanwhile, cyclometalated iridium(III) complexes have gained increasing attention in bioimaging and biosensing due to their rich photophysical properties, e.g., high quantum yields, large Stokes shifts, long-lived phosphorescence, and good photostability.[9] Iridium(III) complexes are also good candidates as two-photon absorption (TPA) materials and luminophores.[10] TPA materials that can be excited by near-infrared light (700–1100 nm) have several advantages over conventional one-photon excited staining agents when applied in biosensing and bioimaging, such as decreased photobleaching effects, minimal photodamage of cellular structures, low background interference, and long penetration depth (>500 μm).[11] These advantages make two-photon microscopy an attractive tool to visualize biological events within live cells and intact tissues.[6a,c,12]

Herein, two iridium(III) complexes, **LysoIr1** and **LysoIr2** (Figure 1), were synthesized and developed as one- and two-photon-excited theranostic agents. The photophysical properties, including the pH-dependent phosphorescence, of **LysoIr1** and **LysoIr2** were characterized. Their specificity and photo-

[*] L. He, Dr. C.-P. Tan, R.-R. Ye, Y.-Z. Zhao, Prof. L.-N. Ji, Prof. Dr. Z.-W. Mao
MOE Key Laboratory of Bioinorganic and Synthetic Chemistry
School of Chemistry and Chemical Engineering
Sun Yat-sen University
Guangzhou 510275 (P. R. China)
E-mail: tancaip@mail.sysu.edu.cn
cesmzw@mail.sysu.edu.cn
Y.-H. Liu, Prof. Dr. Q. Zhao
Key Laboratory for Organic Electronics & Information Displays and Institute of Advanced Materials
Nanjing University of Posts & Telecommunications
9 Wenyuan Road, Nanjing 210046 (P. R. China)

[**] This work is supported by the National Natural Science Foundation of China (no. 21172274, 21231007, 21121061, and 21201183), the 973 Program (no. 2014CB845604), the 863 Program (no. 2012AA020305), the Ministry of Education of China (no. IRT1298 and 313058), and the Fundamental Research Funds for the Central Universities. We thank Prof. W.-J. He for his kind assistance in FLIM experiments.

Supporting information for this article is available on the WWW under http://dx.doi.org/10.1002/anie.201407468.

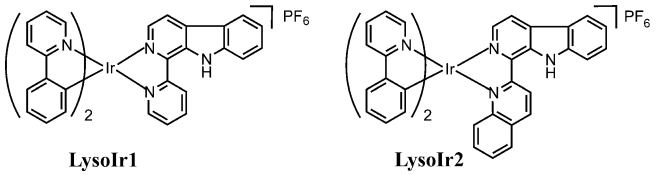

Figure 1. Structures of iridium(III) complexes **LysoIr1** and **LysoIr2**.

stability to label lysosomes were evaluated and their ability to induce autophagy was examined with a variety of methods. Finally, the capability of **LysoIr2** to function as theranostic agents by simultaneously inducing autophagy and tracking autophagic lysosomes was explored.

The synthesis of **LysoIr1** and **LysoIr2** is summarized in the Supporting Information (SI). They were characterized by ^{1}H NMR spectroscopy, ESI-MS, and CHN elemental analysis (for details see SI) as well as X-ray crystallography (Figure S3, Tables S1 and S2). The photophysical data of **LysoIr1** and **LysoIr2** are summarized in Table S3. In disodium hydrogen phosphate/citric acid buffer solutions, the absorption bands at approximately 350–480 nm are assigned to metal-to-ligand charge-transfer (^{1}MLCT) absorption (Figure S4). The maximum emission wavelengths (λ_{em}) are ca. 600 nm and 645 nm for **LysoIr1** and **LysoIr2**, respectively.

The protonation/deprotonation processes, which can perturb the electronic properties of the molecules and result in pH-sensitive fluorescence/phosphorescence properties, are widely recognized mechanisms of many lysosomal trackers.[6e,g,12a] It is found that both **LysoIr1** and **LysoIr2** show pH-sensitive phosphorescence in disodium hydrogen phosphate/citric acid buffer solutions, which is ascribed to the protonation/deprotonation of the secondary amine of the indole rings on the β-carboline ligands (Figure 2 and Figure S5). Under neutral and basic conditions (pH ≥ 7.4), the phosphorescence of **LysoIr1** and **LysoIr2** becomes very weak and "turned-off". When the pH is changed from weakly basic (8.2) to acidic (3.0), a significant increase in the intensity of the phosphorescence, ca. 35- and 30-fold enhancement for **LysoIr1** and **LysoIr2**, respectively, can be observed. Moreover, the pK_a values determined from the sigmoidal curves obtained from recording the phosphorescence intensity at intervals between pH 3.4 and 8.2 are 5.56 and 5.19 for **LysoIr1** and **LysoIr2**, respectively (insets in Figure 2 and Figure S5). These values match the typical pH values of acidic cell organelles.

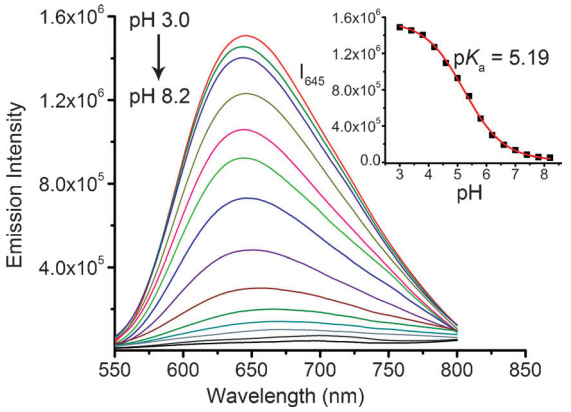

Figure 2. pH-sensitive emission spectra of **LysoIr2** (10 μM, λ_{ex} = 420 nm) in disodium hydrogen phosphate/citric acid buffer solutions. Inset: A plot of emission intensity of **LysoIr2** at 645 nm versus different pH values.

We then evaluated their pH-dependent emission properties in the two-photon mode (Figures S6 and S7). The TPA cross-sections of **LysoIr1** and **LysoIr2** at different pH were determined by investigating their two-photon excited fluorescence (TPEF) using rhodamine 6G as the reference.[13] The maximum TPA cross-sections (δ_{max}, λ_{ex} = 810 nm) were measured to be 958 and 972 GM at pH 3.4 for **LysoIr1** and **LysoIr2**, respectively (Table S3). These values are among the largest TPA cross-sections reported for iridium complexes.[10] The two-photon action cross-section ($\Phi\delta$), the product of the TPA cross-section and fluorescence/phosphorescence quantum yield, can provide direct measure of TPEF brightness and is a more important feature to evaluate the efficiency of two-photon luminophores.[14] The maximum two-photon action cross-sections ($\Phi\delta_{max}$) at pH 3.4, 5.4, and 7.4 are 137, 73, and 5.8 GM for **LysoIr1**, and are 105, 62, and 3.1 GM for **LysoIr2**, respectively (Table S3, Figure S6a and b). The $\Phi\delta_{max}$ values at acidic pH (3.4) are much higher than those reported for commercial probes ($\Phi\delta_{max}$ < 20 GM) and comparable to those reported for typical organic two-photon lysosomal and pH-sensitive probes (16–431 GM).[6a,c,12] **LysoIr1** and **LysoIr2** display ca. 24- and 34-fold higher $\Phi\delta_{max}$ values at pH 3.4 than those obtained at pH 7.4, respectively. Moreover, TPEF spectra of **LysoIr1** and **LysoIr2** show pH-responsive characteristics that are similar to those observed under one-photon excitation (Figure S6c and d).

Cytotoxic assay shows that **LysoIr2** displays lower cytotoxicity than **LysoIr1** against human lung adenocarcinoma A549 cells. The percentage of viable cells is larger than 90% after 3 h incubation with **LysoIr2** (10 μM). Exposure to **LysoIr2** (10 μM) for 6 h causes about 35% reduction in the viability of A549 cells (Figure S8).

As demonstrated above, the pK_a values of **LysoIr1** and **LysoIr2** match the typical pH values of lysosomes, indicating that they are suitable for labeling acidic structures (e.g., lysosomes and endosomes) in cells. Colocalization experiments of **LysoIr1** or **LysoIr2** with commercial LysoTracker Green DND-26 (LTG) in A549 cells under one- and two-photon excitation demonstrates the specific lysosomal staining of the probes (Figure 3 and Figure S9a). Under two-photon excitation, the Pearson's colocalization coefficients of **LysoIr1** and **LysoIr2** with LTG are 0.85 and 0.91, respectively. Meanwhile, little colocalization for **LysoIr1** and **LysoIr2** with MitoTracker Green FM (MTG) is observed, which indicates that **LysoIr1** and **LysoIr2** possess lysosomal specificity (Figures S9b and S10). The specific staining of lysosomes by **LysoIr1** and **LysoIr2** is also confirmed in human breast cancer MCF-7 cells and human cervical cancer HeLa cells (Figures S11–S14).

By using lifetime gating in fluorescence lifetime imaging microscopy (FLIM) applications, **LysoIr1** and **LysoIr2** can image lysosomes in the absence of cellular autofluorescence (Figure S15a, b, d, and e).[15] Additionally, the intracellular

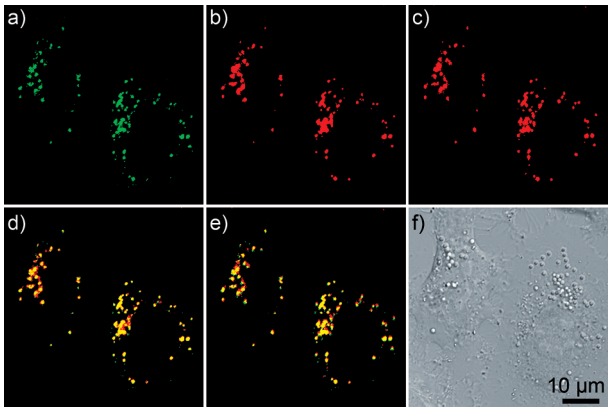

Figure 3. One- and two-photon images of A549 cells co-labeled with **LysoIr2** (10 μM, 1 h) and LTG (150 nM, 0.5 h). a) LTG ($\lambda_{ex}=488$ nm, $\lambda_{em}=511\pm20$ nm). b) One-photon excited **LysoIr2** ($\lambda_{ex}=405$ nm, $\lambda_{em}=645\pm20$ nm). c) Two-photon excited **LysoIr2** ($\lambda_{ex}=810$ nm, $\lambda_{em}=645\pm20$ nm). d) Overlay of (a) and (b). e) Overlay of (a) and (c). f) Bright field.

acidity can also be mapped based on the phosphorescence lifetimes of Ir^{III} (Figure S15c and f). The average phosphorescence lifetimes of **LysoIr1** and **LysoIr2** in cells are determined to be ca. 111 and 140 ns, respectively, which is consistent with the lifetimes of **LysoIr1** and **LysoIr2** at lysosomal pH (Table S3).

The photostability of **LysoIr2** was evaluated by a photobleaching experiment. Under successive irradiation at the same intensity with the help of a power meter, the phosphorescence intensity of **LysoIr2** remains at a level of 60% of the initial phosphorescence intensity after 20 scans (7.75 s per scan; Figure S16). On the other hand, the fluorescence intensity of LTG decreases rapidly to 15% under the same conditions. The high photostability of **LysoIr2** makes it favorable for real-time lysosomal tracking.

Based on our former observations that iridium(III)-β-carboline complexes can induced autophagy in cancer cells,[16] we further investigated whether **LysoIr1** and **LysoIr2** can also induce autophagy in A549 cells. The ultrastructural and morphological alterations in A549 cells upon **LysoIr1** and **LysoIr2** treatment were investigated by transmission electron microscopy (TEM). Most of the Ir^{III}-treated cells were found to display morphological characteristics of autophagy, e.g., extensive vacuoles containing degraded material (Figure 4 and Figure S17a). Microtubule-associated light chain 3 (LC3) protein can specifically label autophagosomal membranes, and the conversion of LC3-I to LC3-II is generally accepted as an autophagy marker.[17] Western blotting analysis shows that the ratio of LC3-II/LC3-I is markedly increased after **LysoIr1** and **LysoIr2** treatment as compared with the vehicle-treated control, which is similar to that observed for the established autophagy inducer rapamycin (Figure S17b). Accordingly, eGFP-LC3 localization study shows that the protein is distributed diffusely (LC3-I) in vehicle-treated A549 cells, whereas most of the cells treated with rapamycin (72.1 ± 4.5%), **LysoIr1** (73.2 ± 5.7%), or **LysoIr2** (77.0 ± 6.9%) display an intense punctate pattern (LC3-II; Figure S17c and d).

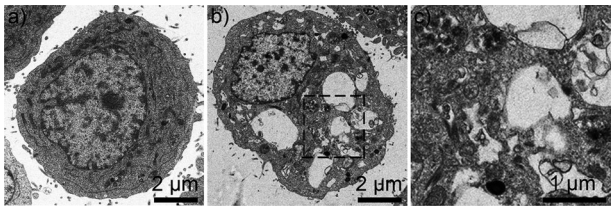

Figure 4. Representative TEM images showing the morphological features of A549 cells treated with a) vehicle control and b) **LysoIr2** (4 μM) for 24 h. c) Magnified view of the black box region in (b).

As a real-time lysosomal tracker, **LysoIr2** is more suitable compared with **LysoIr1** because of its longer emission wavelength, a pK_a value closer to the lysosomal pH, higher Pearson's colocalization coefficient, and lower cytotoxicity; therefore, **LysoIr2** is chosen for further explorations.

The signaling pathways of autophagy and apoptosis are extensively interconnected.[18] The ability of **LysoIr2** to induce apoptosis in A549 cells was investigated by the annexin V staining assay (Figure S18a and b). Compared with the vehicle-treated control cells (5.3 ± 0.4%), **LysoIr2** treatment causes a negligible increase in the percentage of annexin V-positive A549 cells (2 μM: 5.7 ± 0.8%; 4 μM: 6.7 ± 0.7%; 8 μM: 7.9 ± 0.9%). However, a considerable percentage of cells undergo apoptosis upon cisplatin treatment (25 μM: 32.3 ± 3.1%; 50 μM: 49.1 ± 3.8%). Consistent with these observations, the activity of caspase-3/7, key executioners of apoptosis, does not increase upon **LysoIr2** (4 μM) treatment, whereas cisplatin (50 μM) causes an approximately 2.4-fold increase in caspase-3/7 activity (Figure S18c). These results reveal that **LysoIr2** mainly induces autophagy, but not apoptosis, in A549 cells.

As demonstrated above, **LysoIr2** can induce autophagy in A549 cells, and it is also a very specific lysosomal probe that is suitable for real-time lysosomal tracking. We conceived that **LysoIr2** could be utilized to monitor the alternations of lysosomal morphology in real-time during autophagic processes. As the treatment time increases, the enlargement of the total volume of acidic compartments is unambiguously indicated by the red fluorescence from **LysoIr2** (10 μM) under both one- and two-photon excitation (Figure 5 and Figure S19, Movies S1 and S2).

Furthermore, the fusion of mature autophagosome with endosome/lysosome to form autolysosome for degradation of

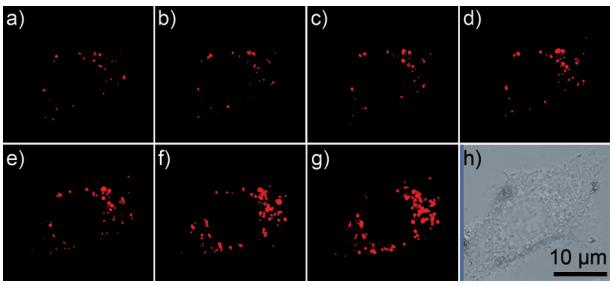

Figure 5. Two-photon excited real-time tracking of lysosomes in A549 cells stained with **LysoIr2** (10 μM) at 37°C for different time intervals. a) 0.25 h, b) 0.5 h, c) 1 h, d) 1.5 h, e) 2 h, f) 4 h, g) 6 h, and h) bright field.

its contents is a crucial stage of autophagy.[7] Since **LysoIr2** can induce autophagy and monitor lysosomes in real-time, it can be used to study the interactions of lysosomes with other labeled biological molecules/organelles during autophagic processes. To demonstrate the effectiveness of our proposal, eGFP-LC3-transfected A549 cells were treated with **LysoIr2** (10 μM) and monitored by confocal microscope under both one- and two-photon excitation (Figure 6 and Figure S20). After ca. 30 min, small eGFP-LC3 dots gradually emerged,

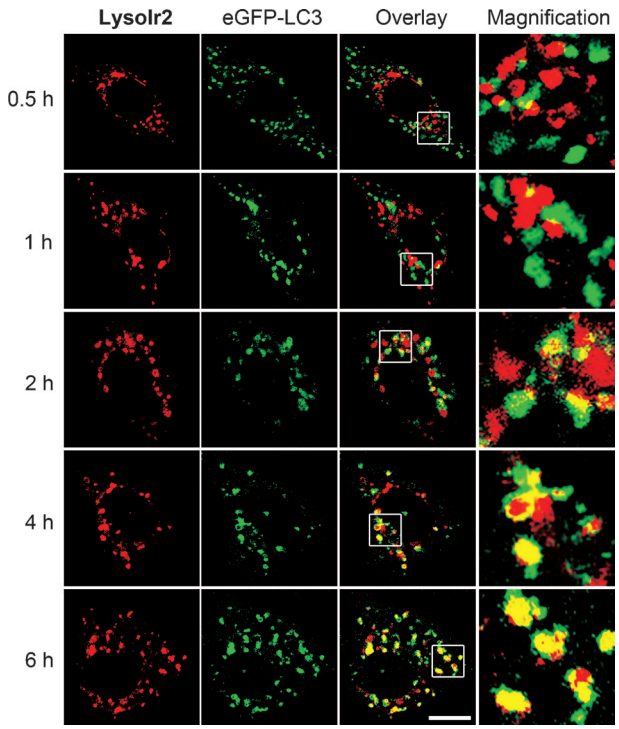

Figure 6. Visualization of autophagosomal–lysosomal fusion by **LysoIr2** (10 μM) under two-photon excitation. A549 cells transfected with eGFP-LC3 were treated with **LysoIr2** for the indicated time intervals and then imaged by confocal microscopy. **LysoIr2**: $\lambda_{ex} = 810$ nm, $\lambda_{em} = 645 \pm 20$ nm; eGFP-LC3: $\lambda_{ex} = 488$ nm; $\lambda_{em} = 510 \pm 20$ nm. Scale bar: 10 μm.

while negligible colocalization of green dots and red dots can be detected. When the treatment time is extended to 1–2 h, there is an increase in both number and size of eGFP-LC3 puncta, and the Pearson's colocalization coefficient of lysosomes and autophasosomes increases to about 0.36 (Figure S21). After 6 h of **LysoIr2** treatment, a higher Pearson's colocalization coefficient (0.65) is observed, indicating that a substantial number of eGFP-LC3 puncta are merged with lysosomes. These data clearly demonstrate that **LysoIr2** can effectively implement two functions, namely autophagy induction and lysosomal tracking, in the visualization of autophagosomal–lysosomal fusion.

In summary, we have developed two iridium(III) complexes that can specifically image lysosomes and induce an autophagic response in live cells. These two features make them ideal probes to track autophagic lysosomes. We show that **LysoIr2** allows specific visualization of lysosomes during the autophagic process in live cells without any additional labeling operations. Thus, **LysoIr2** can greatly simplify the staining procedures to study the key events in autophagy associated with lysosomes, e.g., autophagosomal–lysosomal fusion. More importantly, **LysoIr1** and **LysoIr2** display marked TPA and emission properties, which can greatly enhance their sensitivity and expand their compatibility with other staining methods by minimizing the interference with the background noises and other labeling agents. We consider that **LysoIr2** can be utilized as a useful research tool to track autophagic lysosomes in real-time.

Received: July 22, 2014
Revised: August 19, 2014
Published online: September 22, 2014

Keywords: autophagy · bioinorganic chemistry · iridium · probe · theranostic

[1] a) P. Saftig, J. Klumperman, *Nat. Rev. Mol. Cell Biol.* **2009**, *10*, 623–635; b) G. Kroemer, M. Jaattela, *Nat. Rev. Cancer* **2005**, *5*, 886–897; c) M. E. Guicciardi, M. Leist, G. J. Gores, *Oncogene* **2004**, *23*, 2881–2890.
[2] a) N. Mizushima, B. Levine, *Nat. Cell Biol.* **2010**, *12*, 823–830; b) E. White, *Nat. Rev. Cancer* **2012**, *12*, 401–410.
[3] N. Mizushima, *Genes Dev.* **2007**, *21*, 2861–2873.
[4] H. M. Shen, N. Mizushima, *Trends Biochem. Sci.* **2014**, *39*, 61–71.
[5] a) L. Yu, C. K. McPhee, L. Zheng, G. A. Mardones, Y. Rong, J. Peng, N. Mi, Y. Zhao, Z. Liu, F. Wan, D. W. Hailey, V. Oorschot, J. Klumperman, E. H. Baehrecke, M. J. Lenardo, *Nature* **2010**, *465*, 942–946; b) T. E. Rusten, K. Lindmo, G. Juhasz, M. Sass, P. O. Seglen, A. Brech, H. Stenmark, *Dev. Cell* **2004**, *7*, 179–192.
[6] a) X. Wang, D. M. Nguyen, C. O. Yanez, L. Rodriguez, H. Y. Ahn, M. V. Bondar, K. D. Belfield, *J. Am. Chem. Soc.* **2010**, *132*, 12237–12239; b) S. Yao, H. Y. Ahn, X. Wang, J. Fu, E. W. Van Stryland, D. J. Hagan, K. D. Belfield, *J. Org. Chem.* **2010**, *75*, 3965–3974; c) H. Yu, Y. Xiao, L. Jin, *J. Am. Chem. Soc.* **2012**, *134*, 17486–17489; d) J. Fan, H. Dong, M. Hu, J. Wang, H. Zhang, H. Zhu, W. Sun, X. Peng, *Chem. Commun.* **2014**, *50*, 882–884; e) L. Wang, Y. Xiao, W. Tian, L. Deng, *J. Am. Chem. Soc.* **2013**, *135*, 2903–2906; f) Z. Li, Y. Song, Y. Yang, L. Yang, X. Huang, J. Han, S. Han, *Chem. Sci.* **2012**, *3*, 2941–2948; g) Y. M. Ho, N. P. Au, K. L. Wong, C. T. Chan, W. M. Kwok, G. L. Law, K. K. Tang, W. Y. Wong, C. H. Ma, M. H. Lam, *Chem. Commun.* **2014**, *50*, 4161–4163.
[7] a) J. Zhou, S. H. Tan, V. Nicolas, C. Bauvy, N. D. Yang, J. Zhang, Y. Xue, P. Codogno, H. M. Shen, *Cell Res.* **2013**, *23*, 508–523; b) J. Zhou, S. E. Hu, S. H. Tan, R. Cao, Y. Chen, D. Xia, X. Zhu, X. F. Yang, C. N. Ong, H. M. Shen, *Autophagy* **2012**, *8*, 338–349.
[8] a) Z. Liu, I. Romero-Canelon, B. Qamar, J. M. Hearn, A. Habtemariam, N. P. Barry, A. M. Pizarro, G. J. Clarkson, P. J. Sadler, *Angew. Chem. Int. Ed.* **2014**, *53*, 3941–3946; *Angew. Chem.* **2014**, *126*, 4022–4027; b) A. Wilbuer, D. H. Vlecken, D. J. Schmitz, K. Kraling, K. Harms, C. P. Bagowski, E. Meggers, *Angew. Chem. Int. Ed.* **2010**, *49*, 3839–3842; *Angew. Chem.* **2010**, *122*, 3928–3932.
[9] a) K. K. Lo, K. Y. Zhang, S. K. Leung, M. C. Tang, *Angew. Chem. Int. Ed.* **2008**, *47*, 2213–2216; *Angew. Chem.* **2008**, *120*, 2245–2248; b) C. Li, M. Yu, Y. Sun, Y. Wu, C. Huang, F. Li, *J. Am. Chem. Soc.* **2011**, *133*, 11231–11239; c) Y. You, Y. Han, Y. M. Lee, S. Y. Park, W. Nam, S. J. Lippard, *J. Am. Chem. Soc.* **2011**, *133*, 11488–11491; d) Y. You, S. Cho, W. Nam, *Inorg. Chem.* **2014**, *53*, 1804–1815.

[10] a) J. Massue, J. Olesiak-Banska, E. Jeanneau, C. Aronica, K. Matczyszyn, M. Samoc, C. Monnereau, C. Andraud, *Inorg. Chem.* **2013**, *52*, 10705 – 10707; b) W. J. Xu, S. J. Liu, X. Zhao, N. Zhao, Z. Q. Liu, H. Xu, H. Liang, Q. Zhao, X. Q. Yu, W. Huang, *Chem. Eur. J.* **2013**, *19*, 621 – 629; c) C. L. Ho, K. L. Wong, H. K. Kong, Y. M. Ho, C. T. Chan, W. M. Kwok, K. S. Leung, H. L. Tam, M. H. Lam, X. F. Ren, A. M. Ren, J. K. Feng, W. Y. Wong, *Chem. Commun.* **2012**, *48*, 2525 – 2527; d) R. M. Edkins, S. L. Bettington, A. E. Goeta, A. Beeby, *Dalton Trans.* **2011**, *40*, 12765 – 12770; e) L. S. Natrajan, A. Toulmin, A. Chew, S. W. Magennis, *Dalton Trans.* **2010**, *39*, 10837 – 10846.

[11] a) W. R. Zipfel, R. M. Williams, W. W. Webb, *Nat. Biotechnol.* **2003**, *21*, 1369 – 1377; b) F. Helmchen, W. Denk, *Nat. Methods* **2005**, *2*, 932 – 940; c) C. J. Chang, E. M. Nolan, J. Jaworski, K. Okamoto, Y. Hayashi, M. Sheng, S. J. Lippard, *Inorg. Chem.* **2004**, *43*, 6774 – 6779; d) C. Chung, D. Srikun, C. S. Lim, C. J. Chang, B. R. Cho, *Chem. Commun.* **2011**, *47*, 9618 – 9620.

[12] a) H. M. Kim, M. J. An, J. H. Hong, B. H. Jeong, O. Kwon, J. Y. Hyon, S. C. Hong, K. J. Lee, B. R. Cho, *Angew. Chem. Int. Ed.* **2008**, *47*, 2231 – 2234; *Angew. Chem.* **2008**, *120*, 2263 – 2266; b) J. H. Son, C. S. Lim, J. H. Han, I. A. Danish, H. M. Kim, B. R. Cho, *J. Org. Chem.* **2011**, *76*, 8113 – 8116; c) H. J. Kim, C. H. Heo, H. M. Kim, *J. Am. Chem. Soc.* **2013**, *135*, 17969 – 17977; d) Z. Wu, M. Tang, T. Tian, J. Wu, Y. Deng, X. Dong, Z. Tan, X. Weng, Z. Liu, C. Wang, X. Zhou, *Talanta* **2011**, *87*, 216 – 221.

[13] N. S. Makarov, M. Drobizhev, A. Rebane, *Opt. Express* **2008**, *16*, 4029 – 4047.

[14] a) C. Xu, W. Zipfel, J. B. Shear, R. M. Williams, W. W. Webb, *Proc. Natl. Acad. Sci. USA* **1996**, *93*, 10763 – 10768; b) D. R. Larson, W. R. Zipfel, R. M. Williams, S. W. Clark, M. P. Bruchez, F. W. Wise, W. W. Webb, *Science* **2003**, *300*, 1434 – 1436.

[15] a) A. Orte, J. M. Alvarez-Pez, M. J. Ruedas-Rama, *ACS Nano* **2013**, *7*, 6387 – 6395; b) M. Chen, Y. Wu, Y. Liu, H. Yang, Q. Zhao, F. Li, *Biomaterials* **2014**, *35*, 8748 – 8755.

[16] L. He, S.-Y. Liao, C.-P. Tan, Y.-Y. Lu, C.-X. Xu, L.-N. Ji, Z.-W. Mao, *Chem. Commun.* **2014**, *50*, 5611 – 5614.

[17] K.-H. Baek, J. Park, I. Shin, *Chem. Soc. Rev.* **2012**, *41*, 3245 – 3263.

[18] P. Kreuzaler, C. J. Watson, *Nat. Rev. Cancer* **2012**, *12*, 411 – 424.

